MODELING OF LOW FREQUENCY STONELEY WAVE PROPAGATION IN AN IRREGULAR BOREHOLE

by

Kazuhiko Tezuka

JAPEX Research Center
Chiba, 261 Japan

C.H. Cheng

Earth Resources Laboratory
Department of Earth, Atmospheric, and Planetary Sciences
Massachusetts Institute of Technology
Cambridge, MA 02139

and

X.M. Tang

NER Geoscience
Braintree, MA 02184

ABSTRACT

This paper describes a propagator matrix formulation for the problem of the Stoneley wave propagation in an irregular borehole. This is based on a simple one-dimensional theory that is possible for the low frequency Stoneley wave, because it is a guided wave with no geometrical spreading in the borehole. The borehole and the surrounding formation are modeled by multi-layers discretized along the borehole axis, then the propagator matrices at each boundary are calculated. The mass balance boundary condition is introduced to express an interaction of the Stoneley wave at the interfaces which include radius changes.

We have used the method to investigate the reflection and the transmission characteristics of the Stoneley wave with several models. The results are consistent with the results obtained by other existing modeling methods such as the finite difference method and the boundary integral method. The calculation speed is much faster than those of the other methods.

We have applied the method to the field data to simulate the synthetic iso-offset records and have compared them with the actual field records. The results show a good agreement in the major reflections due to the washout zones and an important disagreement in the reflections related to the fractures. This result suggests the possibility of distinguishing the fracture induced reflections from others.

Through this study, we found that the proposed method is efficient in modeling the low frequency Stoneley wave propagation in the irregular borehole, especially in simulating the synthetic iso-offset records, which provide helpful information in the evaluation of fractures.

INTRODUCTION

The valuation of fractures and associated permeable structures is one of the most important work areas in exploration geophysics. Geothermal and petroleum reservoirs are sometimes characterized by the fracture system that rules their oil, gas and steam productivities. Acoustic logging is one of the effective techniques to evaluate the subsurface fractures crossing the borehole. In particular, the Stoneley wave is known as a wave mode sensitive to the fracture and its permeability. When the Stoneley wave propagates across the fracture, it attenuates its amplitude and also generates a reflected wave (Paillet and White, 1982; Hornby et al., 1989). The reflection patterns, which we can easily see on the iso-offset waveform display, give us good information about the fractures. However, the Stoneley wave reflections occur not only because of the fractures but also because of the lithology and borehole diameter changes (Paillet, 1980; Hardin et al., 1987). In many cases, most of the significant reflections seem to be generated by the borehole washout. To evaluate the fractures by using the Stoneley reflection, it is important to know the effects of the irregular borehole on the Stoneley wave propagation. Stephen et al., (1985) used the finite difference scheme to numerically model such configurations. Bouchon and Schmitt (1988) treated the same problem by using the boundary integral equation approach combining the discrete wavenumber formulation. They showed that when the change is smooth the Stoneley wave propagation was not affected, but a significant amount of reflection could be seen in the case of steep variation. However, these methods are rather time consuming in simulating an actual borehole geometry for practical use. Tang and Cheng (1993) studied the interactions of the Stoneley wave due to the formation structure changes with a simple 1-D theorem. They assumed that the Stoneley wave propagated along the borehole with no geometric spreading because it is a guided wave. We expand their method in order to simulate the Stoneley wave propagation in the irregular borehole which has a variation in borehole radius.

In this paper, we formulate first the basic theory by using the 1-D wave propagation theorem. The reflection and the transmission coefficients due to the change of borehole radius are discussed under two different types of boundary conditions. Then, we expand the theory to treat more complicated borehole geometries by using the propagator matrix. The pressure wavefields inside the borehole are calculated for several cases. Those results are compared with the synthetic waveforms obtained by other modeling methods such as the finite difference method and the boundary integral method. Finally, we apply the method to field data to simulate the reflections due to the washout zones, and also to distinguish these from those due to the fractures.

BASIC THEORY

For the most simple case, we consider a fluid filled borehole surrounded by two layered elastic formations which include one boundary between the upper and the lower half spaces (Figure 1). Each layer is described by its parameters: compressional velocity (v_p), shear velocity (v_s) and density (ρ). The borehole has a step change in radius at the boundary $z = z_1$ and the radius r_i is constant in each layer. The logging tool is simulated as a rigid cylinder of radius r_t at the borehole center. We assume the logging is performed at frequencies below the cut-off frequency of any mode other than the fundamental, so that only the Stoneley wave is supposed to be excited in the borehole. As the Stoneley wave is a kind of guided wave, most of the energy is trapped inside the borehole. There is almost no geometrical spreading, and at such a low frequency, borehole fluid may be considered as approximately uniform across the fluid annulus between the tool and the borehole wall (Tang and Cheng, 1993). Under these conditions it is sufficient to solve the problem as a case of one dimensional wave propagation.

The wave equation for the Stoneley wave is given in terms of displacement potentials.

$$\frac{\partial^2 \phi_i}{\partial z^2} + {k_i}^2 \phi_i = 0 \tag{1}$$

where ϕ_i is the Stoneley wave displacement potential and k_i is the axial Stoneley wavenumber in each layer. The fluid pressure P and the axial displacement u of the Stoneley wave are given by

$$P = \rho_f \omega^2 \phi \tag{2}$$

$$u = \frac{\partial \phi}{\partial z} \tag{3}$$

where ρ_f is a fluid density and ω is an angular frequency.

The solution to Equation (1) is given by

$$\phi_i = D_i e^{ik_i z} + U_i e^{-ik_i z} \tag{4}$$

where D_i and U_i are unknown coefficients at each layer. The first term of Equation (4) represents the down-going wave and the second term represents the up-going wave. Let us consider a down-going Stoneley wave $D_1 e^{ik_1 z}, (z < z_1)$ incident at the boundary. In the upper layer, there are both incident and reflected waves, since some part of the energy of the incident wave will be reflected back from the boundary. Therefore, the potential in the upper layer is given by

$$\phi_1 = D_1 e^{ik_1 z} + U_1 e^{-ik_1 z}$$

where D_1 and U_1 are the amplitude coefficients for the incident and the reflected waves, respectively.

In the lower layer, there are only transmitted waves but no up-going waves because the lower layer is an infinite half space and there is no source.

$$\begin{aligned} \phi_2 &= D_2 e^{ik_2 z} + U_2 e^{-ik_2 z} \\ &= D_2 e^{ik_2 z} \end{aligned}$$

where D_2 is the amplitude coefficient of the transmitted wave. The two unknown coefficients U_1 and D_2 are determined from the boundary conditions.

The coupling inside the borehole is caused by the differences among the k_i propagation constants due to the fact that the property of each layer is different from the other. In addition to the propagation constants the change in the borehole radius is supposed to be a cause of interaction. Then, we consider two sets of boundary conditions. One is a combination of the continuity of the fluid pressure and the continuity of the vertical displacement. Another is a combination of the continuity of the fluid pressure and the fluid mass balance across the boundary. The mass balance means that the volume of the fluid squeezed from the upper layer should be equal to the volume of the incoming fluid in the lower layer. That is

$$a_1 u_1(z_1) = a_2 u_2(z_1) \tag{5}$$

where a_1 and a_2 are section areas of each layers; $u_1(z_1)$ and $u_2(z_1)$ are vertical displacements at $z = z_1$ given by Equation (3). The mass balance condition cannot coincide with the continuity of vertical displacement except for the case of $a_1 = a_2$. Thus, we first solved the amplitude coefficient in two ways by using both sets of boundary conditions independently. Then, both results are discussed by comparing them with the result obtained by other modeling methods later. We shall call the first condition "the non mass balance condition" and the second one "the mass balance condition".

The mass balance condition provides the following simultaneous equations through Equation (5), Equation (2), and Equation (3)

$$\begin{aligned} D_1 e^{ik_1 z_1} + U_1 e^{-ik_1 z_1} &= D_2 e^{ik_2 z_1} \\ a_1 k_1 (D_1 e^{ik_1 z_1} - U_1 e^{-ik_1 z_1}) &= a_2 k_2 D_2 e^{ik_2 z_1}. \end{aligned}$$

These equations can be solved for unknown coefficients U_1 and D_2.

$$\begin{aligned} U_1 &= \frac{a_1 k_1 - a_2 k_2}{a_1 k_1 + a_2 k_2} e^{2ik_1 z_1} D_1 \\ D_2 &= \frac{2a_1 k_1}{a_1 k_1 + a_2 k_2} e^{i(k_1 - k_2) z_1} D_1. \end{aligned} \tag{6}$$

At $z = 0$ the reflection (R) and transmission (T) coefficients are given by

$$\begin{aligned} R = U_1/D_1 &= \frac{a_1 k_1 - a_2 k_2}{a_1 k_1 + a_2 k_2} \\ T = D_2/D_1 &= \frac{2a_1 k_1}{a_1 k_1 + a_2 k_2}. \end{aligned} \tag{7}$$

For the non mass balance condition, another set of simultaneous equations are obtained as

$$\begin{aligned} D_1 e^{ik_1 z_1} + U_1 e^{-ik_1 z_1} &= D_2 e^{ik_2 z_1} \\ k_1 (D_1 e^{ik_1 z_1} - U_1 e^{-ik_1 z_1}) &= k_2 D_2 e^{ik_2 z_1}. \end{aligned}$$

The reflection and the transmission coefficients are given by

$$\begin{aligned} R = U_1/D_1 &= \frac{k_1 - k_2}{k_1 + k_2} \\ T = D_2/D_1 &= \frac{2k_1}{k_1 + k_2}. \end{aligned} \tag{8}$$

It is explicit that both coefficients of the mass balance condition are the same as those of the non mass balance condition if the radius is constant ($a_1 = a_2$).

The wavenumber k of the Stoneley wave in the fluid-filled borehole, surrounded by an elastic formation and containing a rigid tool at the borehole center, is determined by the following borehole period equation (Tang and Cheng, 1991; Schmitt, 1988).

$$\begin{aligned} &\frac{I_0(fr)}{I_1(fr)} + \frac{I_1(fr_t)}{I_1((fr)}\frac{K_0(fr)}{K_1((fr_t)} + \left\{1 - \frac{I_1(fr_t)}{I_1((fr)}\frac{K_1(fr)}{K_1((fr_t)}\right\} \\ &\times \frac{\rho}{\rho_f}\frac{f}{l}\left[(\frac{2v_s^2}{c^2} - 1)^2\frac{K_0(lr)}{K_1((lr_t)} - \frac{2v_s^2 lm}{c^2k^2}\left\{\frac{1}{mr} + \frac{2v_s^2}{c^2}\frac{K_0(mr)}{K_1((mr)}\right\}\right] = 0 \end{aligned} \tag{9}$$

where I_n and K_n are the first and second kind modified Bessel functions of order n ($n = 0, 1$), ρ is formation density, ρ_f is fluid density, $c = \omega/k$ is the Stoneley wave phase velocity and r and r_t are the borehole and tool radii respectively. The radial wavenumbers, l, m and f are given by

$$\begin{aligned} l &= \sqrt{k_2 - \omega_2/v_p^2} \\ m &= \sqrt{k_2 - \omega_2/v_s^2} \\ f &= \sqrt{k_2 - \omega_2/v_f^2}. \end{aligned}$$

For given respective elastic properties of the layer the Stoneley wavenumber k can be determined as a function of frequency.

Figure 2 shows the transmission and the reflection coefficients at the single boundary calculated from Equation (7) and Equation (8). The parameters used in the calculation are: $\rho_1 = 2.6\text{g/cm}^3$, $v_{p1} = 5.0$ km/s, and $v_{s1} = 3.0$km/s for the upper formation and $\rho_2 = 2.3\text{g/cm}^3$, $v_{p1} = 3.0$km/s, and $v_{s1} = 2.7$km/s for the lower formation. The borehole fluid density and velocity are 1.0 g/cm^3 and 1.5km/s. The radii of the borehole in the upper and the lower formation are 0.1m and 0.15m, respectively. The tool radius is $r_t = 0$m. The transmission and the reflection coefficients are calculated for both boundary conditions at frequencies ranging up to 5kHz. The plotted values are the absolute value of the complex coefficients. It is obvious from the figure that the reflection coefficients of the mass balance condition are much larger than those of the non mass balance condition. Inversely, the transmission coefficients of the mass balance condition are smaller than those of the non mass balance condition. The slight inclination of the coefficients curves is due to the dispersion characteristics of the Stoneley wave.

The effect of the radius ratio (r_2/r_1) on both coefficients is shown in Figure 3. The model used in the calculation is depicted in the figure. Only the ratio of the radius of the borehole is changed to 3.0 from 1.0 in the homogeneous formation. In

the mass balance condition, both of the coefficients have a notable dependency on the radius ratio. The reflection coefficient increases with the increasing radius ratio, and the transmission coefficient decreases reversely. Both curves are very much as expected. In the non mass balance condition, however, the reflection coefficients are almost zero. Any changes in both coefficients cannot be seen in the curves. They are insensitive to the change of radius ratios. The two different types of boundary condition result in quite different reflection characteristics. Then, we have the question which boundary condition is proper. A good approach to the discussion of this problem is to calculate the synthetic waveforms and compare them with the results obtained by some other modeling techniques, such as the finite difference method and boundary integral method.

To calculate the synthetic waveforms, we need the Stoneley incident amplitude $A(\omega)$ which is related to the source and the excitation function. At the source position, it is given by

$$A(\omega) = S(\omega)E(\omega) \tag{10}$$

where $S(\omega)$ is the source spectrum and $E(\omega)$is the Stoneley wave excitation function that is given by Tang and Cheng (1993). The excitation function of the Stoneley wave is a function that depends on the formation and fluid properties, and on borehole radius and the tool radius. This function is calculated basically by a discrete wavenumber summation technique; however we are interested in only the Stoneley but not other modes, so that the excitation function can be calculated by the residue theorem (Kurkjian,1985). Putting $D_1(\omega) = A(\omega)$, using the solved amplitude coefficients ($U_i(\omega)$, $D_i(\omega)$), the fluid pressure (from Equation (2) and Equation (3)) in specific receiver positions is calculated as a function of the frequency. The results are then transformed into the time domain using an inverse Fourier transform.

$$\begin{aligned} D(t,z) &= \frac{1}{2\pi}\int_{-\infty}^{\infty} P(\omega,z)e^{i\omega t}d\omega \\ &= \frac{\rho_f}{2\pi}\int_{-\infty}^{\infty} \omega^2\phi(\omega,z)e^{i\omega t}d\omega \end{aligned}$$

Figure 4 shows the synthetic array waveforms of the Stoneley wave propagating across a single boundary. The model and its parameters used in the calculation are the same as those in Figure 2. The Kelly source with the center frequency of 2 kHz is excited at 1.65m above the interface. The seismograms recorded at an array of 30 receivers located along the borehole axis at distances ranging from 0.1m to 3.0m from the source are displayed. The borehole geometry is depicted beside the waveform arrays. In the mass balance case, a remarkable up-going reflection wave is generated at the boundary. Accordingly, the transmitted wave decreases its amplitude below the boundary. In the non mass balance case, however, we can see neither a reflection nor an attenuation at the boundary. Figure 5 shows the synthetic array waveforms obtained by the finite difference method. The waveforms are calculated by using a velocity-stress formulation on a staggered grid (Virieux, 1986; Kostek, 1990; Cheng, 1992). The parameters and the model geometry used in the calculation are the same as those in Figure 4. A 150*250 grid with $\Delta r = \Delta z = 0.02$ m is used. The time step is set at 2μsec. A Kelly source (Kelly et al., 1986) with a center frequency of 2 kHz is applied as source. In the results, we can see a significant reflection at the boundary. The strength of the

reflected waves is the same as that of the reflections we have gotton in the modeling of the mass balance boundary condition (Figure 4)(a). Including the velocity of the Stoneley wave and the process of phase changes at the boundary, the overall features of both results are in quite good agreement. These results lead to the understanding that the mass balance boundary condition provides a more adequate formula than the non mass balance boundary condition to simulate the Stoneley wave propagating across a boundary with borehole radius changes. Thus, we will adopt the mass balance condition for further study.

MULTI LAYERED CASES

We next consider the borehole with various radii in the multi-layered medium. We assume a model of n-1 layers sandwiched between the upper and lower infinite half spaces shown in Figure 6. Each layer is described by its parameter shown in the figure. The displacement potential within each layer is expressed by Equation (4). With the mass balance boundary condition, the amplitude coefficients satisfy the following relation at the boundary.

$$\begin{pmatrix} U_i \\ D_i \end{pmatrix} = M_i \begin{pmatrix} U_{i+1} \\ D_{i+1} \end{pmatrix} \tag{11}$$

where M_i is the propagator matrix given by

$$M_i = \begin{pmatrix} m_{11} & m_{12} \\ m_{21} & m_{22} \end{pmatrix}$$

where

$$\begin{aligned} m_{11} &= \frac{a_i k_i + a_{i+1} k_{i+1}}{2 a_i k_i} e^{i(k_i - k_{i+1}) z_i} \\ m_{12} &= \frac{a_i k_i - a_{i+1} k_{i+1}}{2 a_i k_i} e^{i(k_i + k_{i+1}) z_i} \\ m_{21} &= \frac{a_i k_i - a_{i+1} k_{i+1}}{2 a_i k_i} e^{-i(k_i + k_{i+1}) z_i} \\ m_{22} &= \frac{a_i k_i + a_{i+1} k_{i+1}}{2 a_i k_i} e^{-i(k_i - k_{i+1}) z_i}. \end{aligned} \tag{12}$$

We assume a unit impulse incident wave onto the interface $z = z_1$ from the upper half space. The coefficient of the down-going wave in the upper half space D_1 is supposed to be 1. Successive application of Equation (11) and additional use of the relation $U_n = 0$ (no up-going waves in the lower half space) yield

$$\begin{aligned} \begin{pmatrix} U_1 \\ D_1 \end{pmatrix} &= M_1 \begin{pmatrix} U_2 \\ D_2 \end{pmatrix} \\ &= M_1 M_2 \cdots M_{n-1} \begin{pmatrix} 0 \\ D_n \end{pmatrix} \\ &= M_T \begin{pmatrix} 0 \\ D_n \end{pmatrix} \end{aligned}$$

with the multiple propagator matrix product

$$M_T = \prod_{i=1}^{n-1} M_i = \begin{pmatrix} m_{T11} & m_{T12} \\ m_{T21} & m_{T22} \end{pmatrix}. \tag{13}$$

Then the unknown coefficients U_1 and D_n can be given by

$$\begin{pmatrix} U_1 \\ D_n \end{pmatrix} = W_T \begin{pmatrix} 0 \\ D_1 \end{pmatrix}$$
$$D_1 = 1$$

where

$$W_T = \frac{1}{m_{T22}} \begin{pmatrix} m_{T11}m_{T22} - m_{T12}m_{T21} & m_{T12} \\ -m_{T21} & 1 \end{pmatrix}. \tag{14}$$

U_1 is the amplitude coefficient of the reflected Stoneley wave in the upper half space, and D_n is that of the transmitted Stoneley wave in the lower half space. Once we know D_n and $U_n = 0$, we can solve U_{n-1}, D_{n-1} and $U_{n-2}, D_{n-2} \cdots$ successively up to U_2, D_2 by using Equation (11).

Let us consider the Stoneley propagation across a simple rectangular washout zone sandwiched between two infinite half space formations of the same properties. Using Equation (12) to Equation (14), putting $n = 3$, $z_1 = 0$, and $z_2 = L$ the total transmission and reflection coefficients from the washout zone whose thickness of L are given by

$$T = D_3/D_1 = \frac{4a_1a_2k_1k_2e^{-ik_1L}}{G}$$
$$R = U_1/D_1 = \frac{2i(a_2^2k_2^2 - a_1^2k_1^2)\sin(k_2L)}{G} \tag{15}$$

where the denominator $G(\omega)$ is given by

$$G = (a_1K_1 + a_2k_2)^2e^{-ik_2L} - (a_1k_1 - a_2k_2)^2e^{ik_2L}.$$

Figure 7 shows the total transmission (a) and reflection (b) curves of the Stoneley wave. The parameters and the borehole geometry used for the calculation are depicted in the figure. The figures plot the amplitude of both the total coefficients versus frequency for two different zone thicknesses. They are $L = 0.5m$ and $L = 0.1m$. As the total reflection coefficient comes mainly from the superposition of the two primary reflected up-going waves (at $Z = 0$ and $z = L$), it shows a periodic spectrum that contains a number of maxima and minima (Tang and Cheng, 1993). The period of the maxima or minima, that is approximately a function of the averaged Stoneley velocity and the zone thickness (L), is inversely proportional to L. If the center frequency of the Stoneley wave is close to the frequency corresponding to the minima, the reflection is small, even if there are significant radius changes. The superpositions of the primary reflections from the several boundaries are essentials characterizing the total reflection from the complicated borehole geometry. Figure 8 shows the total reflection (R) and transmission (T) coefficient at the sinusoidal washout zone. The washout zone is discretized with 100 layers. The borehole radii of the layers vary sinusoidally giving the characteristic bulge at the washout zone. The parameters used in the calculation are the same as

Figure 7. The coefficients calculated for three different zone thicknesses (L=0.1m, 0.2m and 0.5m) are plotted against frequency. The total reflection coefficients depend strongly on the frequency. They have peaks at specific frequencies that are a function of zone thicknesses. The peak frequency shifts to the lower, and the band width of the spectrum becomes narrower with increasing zone thickness. In the case of the smooth varied washout zone (L=0.5m), only the limited low frequency Stoneley wave will be reflected. The periodic bumps in the spectrum (R0.5) come from the superpositions we mentioned before.

COMPARISON WITH THE BOUNDARY INTEGRAL MODELING

Bouchon and Schmitt (1989) studied the Stoneley wave propagation in an irregular borehole by using the boundary integral equation combining the discrete wavenumber formulation. This is a semi-analytical approach. They reported that a smooth variation in a borehole radius does not effect the records obtained ahead of the discontinuity location, but that the presence of steep radius discontinuity reflects a significant amount of the Stoneley energy. To confirm the performance of our new method, we apply it to the steep radius variation model and to the smooth radius variation model used in Bouchon and Schmitt's study.

The steep model has an interval whose radius changes sinusoidally from 12cm at an axial distance of 1.5m from the source to a value of 7cm at a distance of 1.6m. The smooth model has the same change occurring between the distances of 1.0m and 2.0m. The parameters of the formation and the fluid are the same as those in Figure 3 as a source. In the propagator matrix modeling, we finely discretized the transition interval into 100 layers. Putting the infinite half space on the top and at the bottom layer of the interval, a model consist of a total of 102 layers is used for the calculation. A Kelly source with a center frequency of 2 kHz is applied as a source.

Figure 9 shows the sets of waveform arrays obtained by the propagator matrix method and the boundary integral method in the steep model. The source frequency is below the cut-off frequency of any mode other than the fundamental, so that only the Stoneley wave is excited. The results show quite good agreement with each other. The steep change in the borehole radius gives rise to a reflected Stoneley wave. The amplitudes of the reflected waves are almost the same. The velocities of the Stoneley waves are also in good agreement. We can also see good agreement in the results of the smooth model in Figure 10. There can be seen neither reflections nor any perturbations due to the radius changes. Only the amplitude of the Stoneley wave becomes larger gradually from a distance of 1.0m to 2.0m, corresponding to the smooth decrease in radius. We can conclude that the overall features, including the reflection, the transmission, and the velocity characteristics of the propagator matrix modeling are consistent with the boundary integral modeling.

It is promising that the Stoneley wave propagation in the irregular borehole can be modeled by the simple 1-D wave propagation theory with the mass balance boundary condition.

SYNTHETIC ISO-OFFSET RECORDS

Full waveform traces of acoustic logging are sometimes displayed as so called iso-offset records forms, that is an array of traces recorded by fixing the source-receiver distance and moving the tool along the borehole. In the iso-offset records, the reflection event makes a specific pattern of spreading both upward and downward symmetrically. The pattern helps an analyst to recognize the location of the obstacle causing the reflection. In the previous section we described the source in the infinite half spaces. However, to get synthetic iso-offset records, we need to allow the source to be located at any depth in the irregular borehole. In this section, prior to making synthetic iso-offset records, we describe the procedure to treat the source inside the irregular borehole. This problem is analogous to the problem of the sources in the layered medium (Temme and Müller 1982). The geometry of the medium is illustrated in Figure 11. The source is located in the Sth layer at the depth of $z = z_s$. The Sth layer requires special treatment, because there is a stress jump at the source point, and the source potential has to be included in the displacement potential of the Sth layer ϕ_s. We separate the Sth layer into two layers. Above the source ($z < z_s$) we use a new denotation S+ with amplitude coefficient D_{s+}, U_{s+}, and below the source ($z > z_s$) we assign D_{s-}, U_{s-} to the coefficients. The relation between the two pairs of coefficients is

$$\begin{pmatrix} U_{s+} \\ D_{s+} \end{pmatrix} = \begin{pmatrix} U_{s-} \\ D_{s-} \end{pmatrix} + \begin{pmatrix} A_s \\ -1/A_s \end{pmatrix}, \qquad A_s = e^{ik_s z_s} \tag{16}$$

where A_s is the source term. With additional relations of $D_1 = 0$ (no down-going wave in the upper half space) and $U_n = 0$ (no up-going wave in the lower half space), we apply Equation (11) to the layer 1 to $s+$, and layers s- to n separately.

$$\begin{aligned} \begin{pmatrix} U_1 \\ 0 \end{pmatrix} &= M_1 M_2 \cdots M_{s-1} \begin{pmatrix} U_{s+} \\ D_{s+} \end{pmatrix} \\ &= S \begin{pmatrix} U_{s+} \\ D_{s+} \end{pmatrix} \end{aligned} \tag{17}$$

where

$$S = \prod_{i=1}^{s-1} M_i = \begin{pmatrix} s_{11} & s_{12} \\ s_{21} & s_{22} \end{pmatrix}$$

and

$$\begin{aligned} \begin{pmatrix} U_{s-} \\ D_{s-} \end{pmatrix} &= M_s M_{s+1} \cdots M_{n-1} \begin{pmatrix} 0 \\ D_n \end{pmatrix} \\ &= T \begin{pmatrix} 0 \\ Dn \end{pmatrix} \end{aligned} \tag{18}$$

where

$$T = \prod_{i=s}^{n-1} M_i = \begin{pmatrix} t_{11} & t_{12} \\ t_{21} & t_{22} \end{pmatrix}.$$

Substituting Equation (18) into Equation (17) through Equation (16), we get

$$\begin{pmatrix} U_1 \\ 0 \end{pmatrix} = S * T \begin{pmatrix} 0 \\ D_n \end{pmatrix} + S \begin{pmatrix} A_s \\ -1/A_s \end{pmatrix}, \qquad A_s = e^{ik_s z_s}. \tag{19}$$

This equation can be solved for the unknown coefficients U_1 and D_n in term of matrix with source potential.

$$\begin{pmatrix} U_1 \\ D_n \end{pmatrix} = \frac{1}{\eta} \begin{pmatrix} \xi t_{22} & -\xi t_{12} \\ -s_{21} & -s_{22} \end{pmatrix} \begin{pmatrix} A_s \\ -1/A_s \end{pmatrix} \tag{20}$$

where

$$\begin{aligned} \eta &= s_{21}t_{12} + s_{22}t_{22} \\ \xi &= s_{11}s_{22} - s_{12}s_{21} \end{aligned}$$

Once we know U_1 and D_n, the other coefficients can be solved for successively in the same manner as the multi-layered cases. However, this requires some attention. The coefficients in layers n-1 to s- may be solved from the lower layers as

$$\begin{pmatrix} U_i \\ D_i \end{pmatrix} = M_i \begin{pmatrix} U_{i+1} \\ D_{i+1} \end{pmatrix} \tag{21}$$

and, the coefficients in layer 2 to s+ must be solved from the upper layers as

$$\begin{pmatrix} U_{i+1} \\ D_{i+1} \end{pmatrix} = M_i^{-1} \begin{pmatrix} U_i \\ D_i \end{pmatrix} \tag{22}$$

where M_i^{-1} is the inverse matrix at the ith boundary. In the case of the model consisting of many layers, we don't need to handle all the layers to calculate the waveform at a certain depth but we need the appropriate number of layers above and below the source depth. The farther boundary from the source makes the reflection which arrives later. If the arrival time exceeds the window length of our interest, it appears on the trace as a wrap around ghost. To prevent the ghost, the layers beyond the maximum distance should be replaced with the infinite half layers.

APPLICATION

In the following we present synthetic iso-offset records calculated for the borehole model based on the actual field data. The data used in the modeling includes sonic log, density log, and caliper log. The composite log chart in Figure 12 shows compressional and shear slowness, bulk density, and borehole diameter. We discretized those curves by a one foot interval and made a 560-layer model. The mud velocity and density are set to be 1600km/s and 1.5g/cm^3, respectively. We ignore the tool radius. The propagator matrices are calculated at each boundary. The excitation function for the Stoneley mode is calculated in a layer in which the source is posted. Then the synthetic waveforms are obtained by following the procedure described in the preceding section. The Kelly

source with a center frequency of 1.5kHz is applied as the source. The receiver is fixed at 9ft above the source. The source and receiver set is moved from the depth of X292ft up to x098ft.

Figure 13 shows the field records (a) and the synthetic records (b) for the field model. Each trace is plotted at the center depth of the source and the receiver. Two large reflection patterns corresponding to the washout zone are recognized at depth of x113ft and x244ft in the synthetic records. Oddly enough the reflection at the upper washout zone seems smaller than the reflection at the lower washout zone, despite that the upper washout zone is larger than the lower zone. This is because of the shape of the washout zone shown in the borehole geometry depicted beside the iso-offset records. The bottom part of the lower washout zone has a rapid change in the borehole radius as against the smooth shape of the upper washout zone. The rapid change causes the big reflection. We can also see some reflection patterns in the field records, however, the low frequency coherent waves make it difficult to see the amplitudes of the reflected waves. To reduce the contamination of the coherent waves and also to remove the transmitted waves, the median filtering (Hardage, 1983) is applied to both the field and the synthetic records. Figure 14 shows the scattered wavefield of both the field records (a) and the synthetic records (b). The coherent waves on the raw field records and the transmitted wave on both records have been successfully removed. In the field records are seen the large reflections corresponding to the washout zones. The reflection strength associated with the upper washout zone is smaller than that of the upper washout zone and is consistent with the synthetic records. As for the washout zone, both records are in good agreement. However, we also have an interesting disagreement. At the depth of X143ft at which the notable reflection pattern is seen in the field records, we cannot find a similar big event in the synthetic record. There are neither distinctive changes in the borehole geometry nor drastic lithology changes. The reflection seems to be caused by something else, possibly fracture. The left-hand column in Figure 14 shows the fracture density obtained by counting fractures on the resistivity image of the formation micro scanner. There are high density anomalies around the depth of X143ft where the inconsistent reflection has been seen in the field records. There are yet other reflection events only in the field records which correspond to the fracture density anomaly at depths of X190ft and X210ft. These inconsistent reflections are thought to be generated by the fractures crossing the borehole.

It is not easy to discriminate the reflections associated with the fractures from the other reflections on the field records; however, this becomes easier if the synthetic records are introduced. The synthetic records provide the image including only the information related to the borehole geometry and the elastic properties of the formation. The image can be used as helpful background information in the interpretation of fractures by the use of the Stoneley wave reflections.

CONCLUSION

We have formulated a simple modeling method for the Stoneley wave propagation by using the propagator matrix with the mass balance boundary conditions. Applying

the method to some cases, we found that it provides a synthetic pressure field in the borehole which is in good agreement with the results obtained by the finite difference modeling method as well as the boundary integration method.

We have applied the method to the field data and compared the synthetic iso-offset records with the field records. The results show good agreement in the major reflections due to the washout zone, but some significant disagreement in the reflections due to the fracture. Since the synthetic records include only information related to the borehole geometry and the elastic properties of formation, they can be used as helpful background data in distingushing the reflections due to fractures from others.

The calculation speed of the method is much faster than other methods such as the finite difference method and the boundary integral method. This is a great advantage for the application to the field data which requires a big model to synthesize the iso-offset records.

REFERENCES

Bouchon, M., and D.P. Schmitt, 1989, Full-wave acoustic logging in an irregular borehole, *Geophysics, 54,* 758–765.

Cheng, C.H., and M.N. Toksöz, 1981, Elastic wave propagation in a fluid-filled borehole and synthetic acoustic logs, *Geophysics, 46,* 1042–1053.

Cheng, N.Y., Z. Zhu, C.H. Cheng, and M.N. Toksöz, 1992, Experimental and finite difference modeling of borehole mach waves, *M.I.T. Borehole Acoustics and Logging Consortium Annual Report.*

Hardin, E.L., C.H. Cheng, F.L. Paillet, and J.D. Mendelson, 1987, Fracture characterization by means of attenuation and generation of tube waves in fractured crystalline rock at Mirror Lake, New Hampshire, *J. Geophys. Res., 92,* 7989–8006.

Hornby, B.E., D.L. Johnson, K.H. Winkler, and R.A. Plumb, 1989, Fracture evaluation using reflected Stoneley-wave arrivals, *Geophysics, 54,* 1274–1288.

Kelly, K.R., R.W. Ward, and S. Treitel, 1976, Synthetic seismograms: A finite-difference approach, *Geophysics, 41,* 2–27.

Kostek, S., 1990, Modeling of elastic wave propagation in a fluid-filled borehole excited by a piezoelectric transducer, *M.S. Thesis, Massachusetts Institute of technology, Cambridge, Mass.*

Paillet, F.L., and J.E. White, 1982, Acoustic models of propagation in the borehole and their relationship to rock properties, *Geophysics, 47,* 1215–1228.

Paillet, F.L., 1980, Acoustic propagation in the vicinity of fractures which intersect a fluid-filled borehole, *Trans. SPWLA 21st Ann. Symp., Paper DD.*

Stephen, R.A., F. Pardo-Casas, C.H. Cheng, 1985, Finite difference synthetic acoustic

logs, *Geophysics, 50,* 1588–1609.

Schmitt, D.P., 1988, Transversely isotropic saturated porous formations: II. Wave propagation and application to multipole logging, *M.I.T. Full Waveform Acoustic Logging Consortium Annual Report.*

Tang, X.M., and C.H. Cheng, 1993, Effects of a logging tool on the Stoneley wave propagation in elastic and porous formations, *The Log Analysts, 34-5,* 46–56.

Tang, X.M., and C.H. Cheng, 1993, Borehole Stoneley wave propagation across permeable structures, *Geophysical Prospecting, 41,* 165–187.

Temme, P., and G. Müller, 1982, Numerical simulation of Vertical Seismic Profiling, *J. Geophys., 50,* 177–188.

Virieux, J., 1986, P-SV wave propagation in heterogeneous media: velocity-stress finite difference method, *Geophysics, 51,* 889–901.

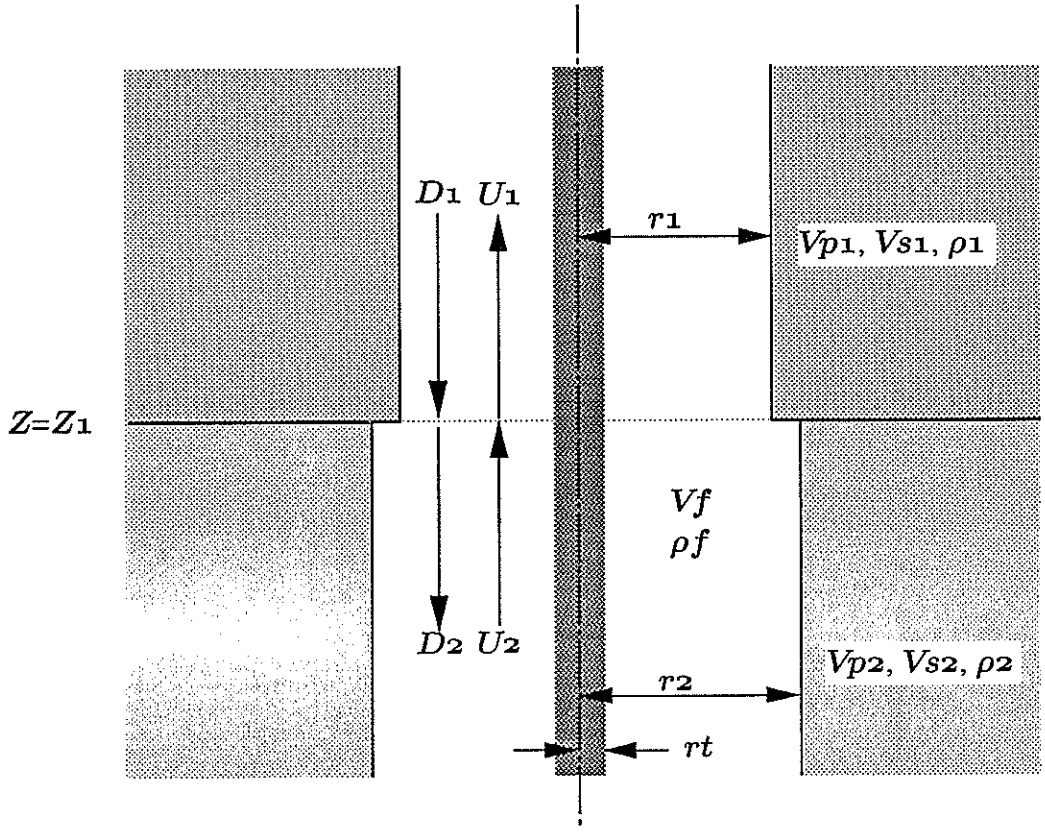

Figure 1: Diagram showing acoustic logging in a formation which has a single boundary between the upper and lower infinite half spaces. Each layer is described by compressional velocity, shear velocity and density. U_i and D_i denote amplitudes of up-going and down-going waves in each layer. A rigid tool is located at the center of the borehole.

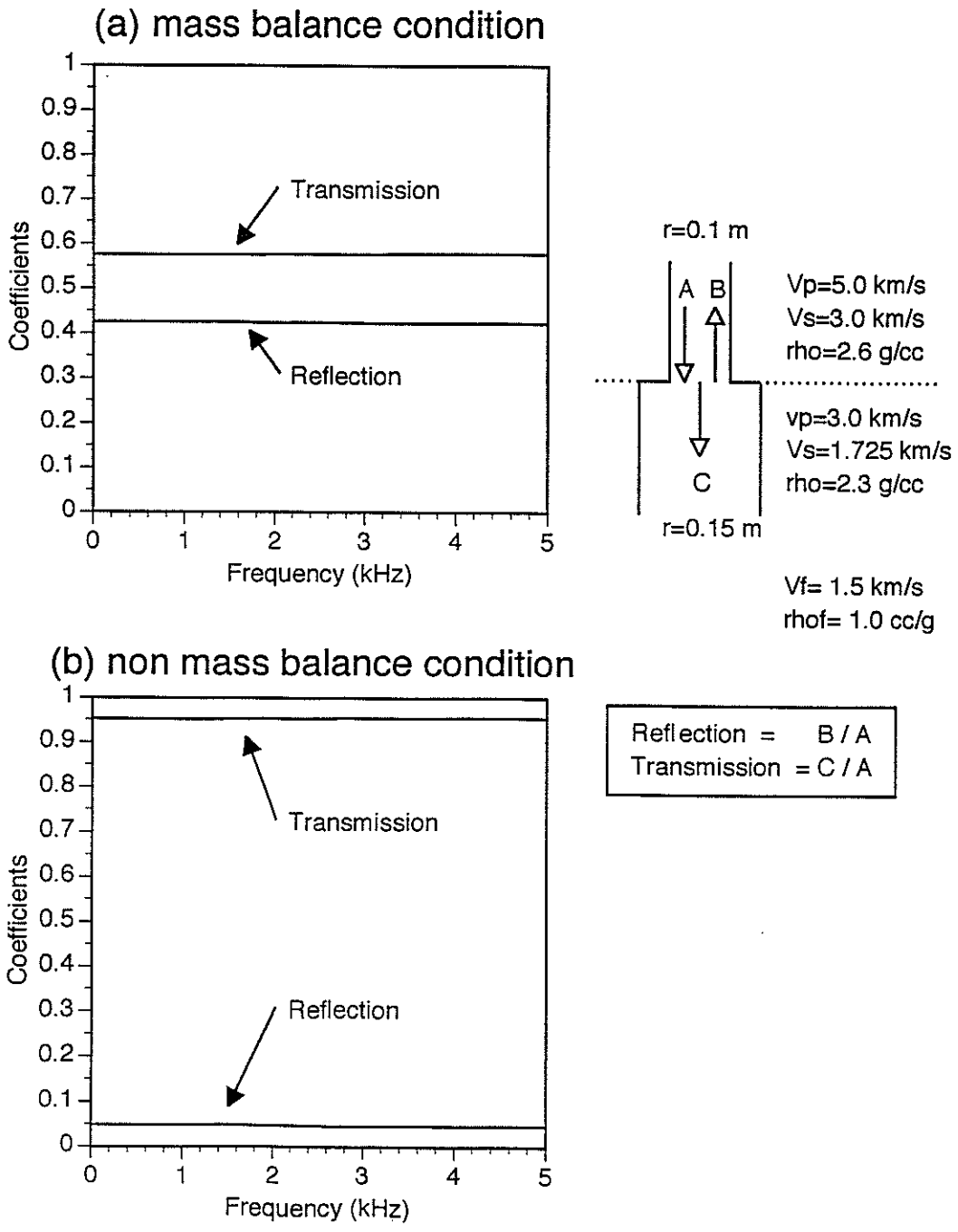

Figure 2: Transmission and reflection coefficients for a Stoneley wave at a single boundary. (a) Results obtained by 'mass balance boundary condition'. (b) Results obtained by 'non mass balance boundary condition'. Borehole geometry and model parameters are depicted beside the curves.

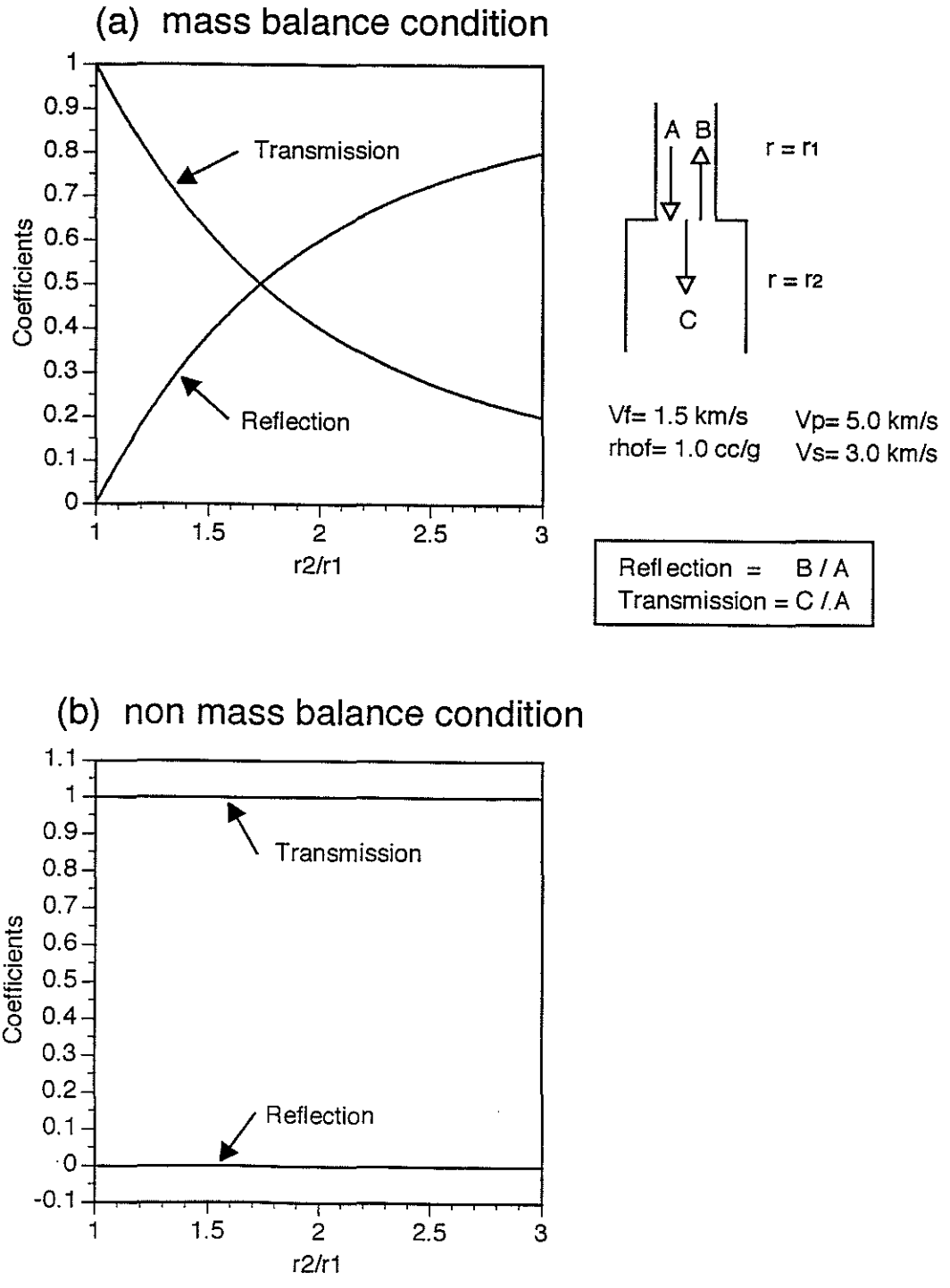

Figure 3: Characteristics of Stoneley reflection and transmission coefficients against ratios of radius changes. (a) Results obtained by 'mass balance boundary condition'. (b) Results obtained by 'non mass balance boundary condition'. Borehole geometry and model parameters are depicted beside the curves.

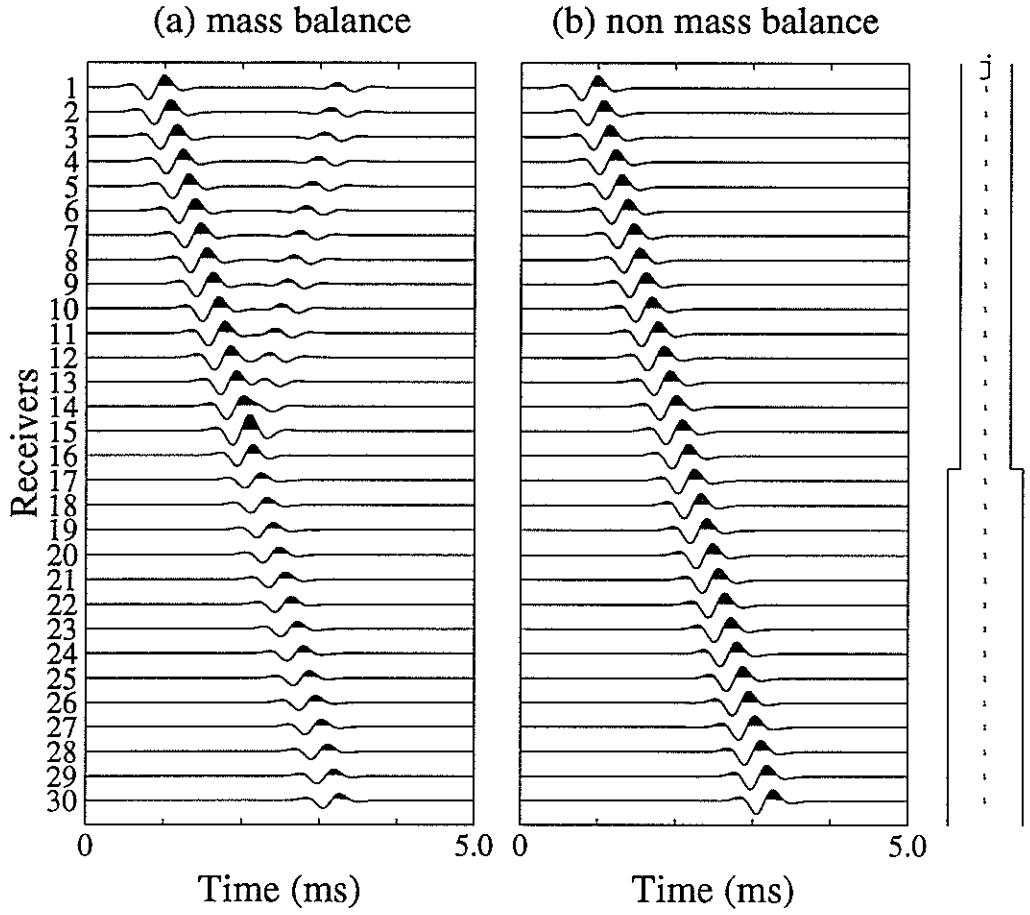

Figure 4: The synthetic array waveforms of the Stoneley wave propagating across a single boundary obtained by the 1-D wave propagation theorem with the 'mass balance boundary condition' (a) and with the 'non mass balance boundary condition' (b). The model parameters used in the calculation are the same as those in Figure 2. The borehole has a step change in radius at 1.65m from the source. The Kelly source with its center frequency of 2 kHz is used for the source function. The seismograms recorded by an array of 30 receivers located along the borehole axis at 0.1m interval are displayed.

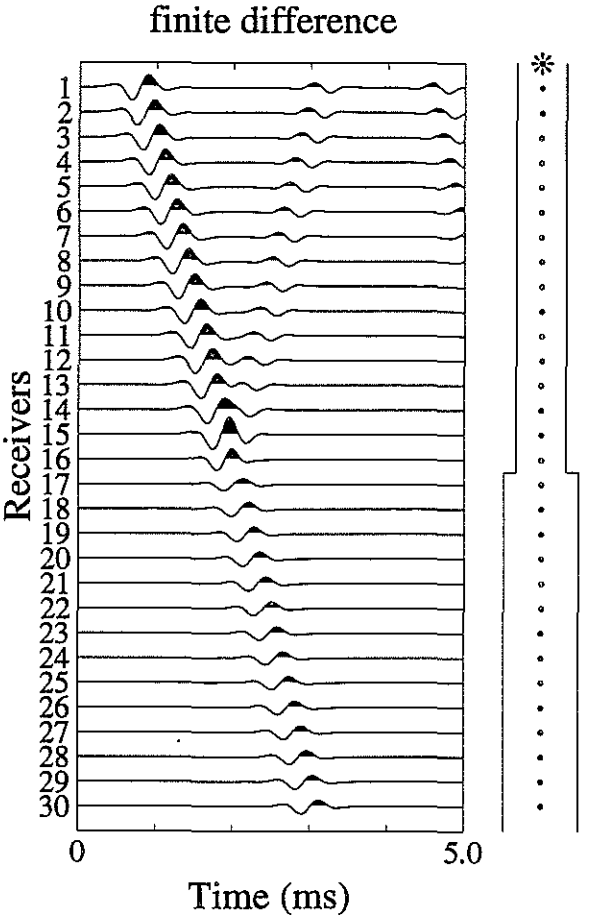

Figure 5: The synthetic array waveforms of the Stoneley wave propagating across a single boundary obtained by the finite difference method. The model parameters used in the calculation are the same as those in Figure 2. The Kelly source with its center frequency of 2 kHz is used for the source function. The seismograms recorded by an array of 30 receivers located along the borehole axis at 0.1m interval are displayed. The reflection and the transmission characteristics are consistent with the results obtained by the 1-D wave propagation theorem with the 'mass balance boundary condition' (Figure 4(a)).

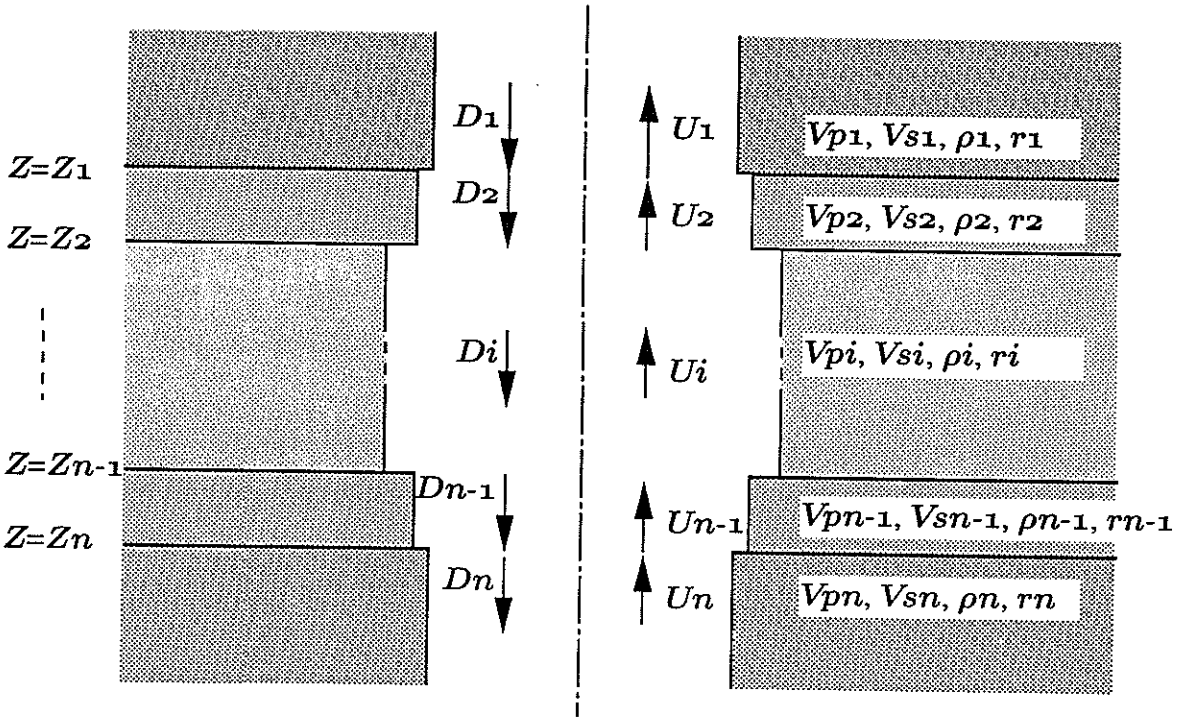

Figure 6: Diagram showing a borehole including washout zone in the multi-layered formation. n-1 layers each of which is described by its parameters and borehole radius are sandwiched between the upper and the lower infinite half spaces. U_i and D_i denote amplitudes of up-going and down-going waves in each layer.

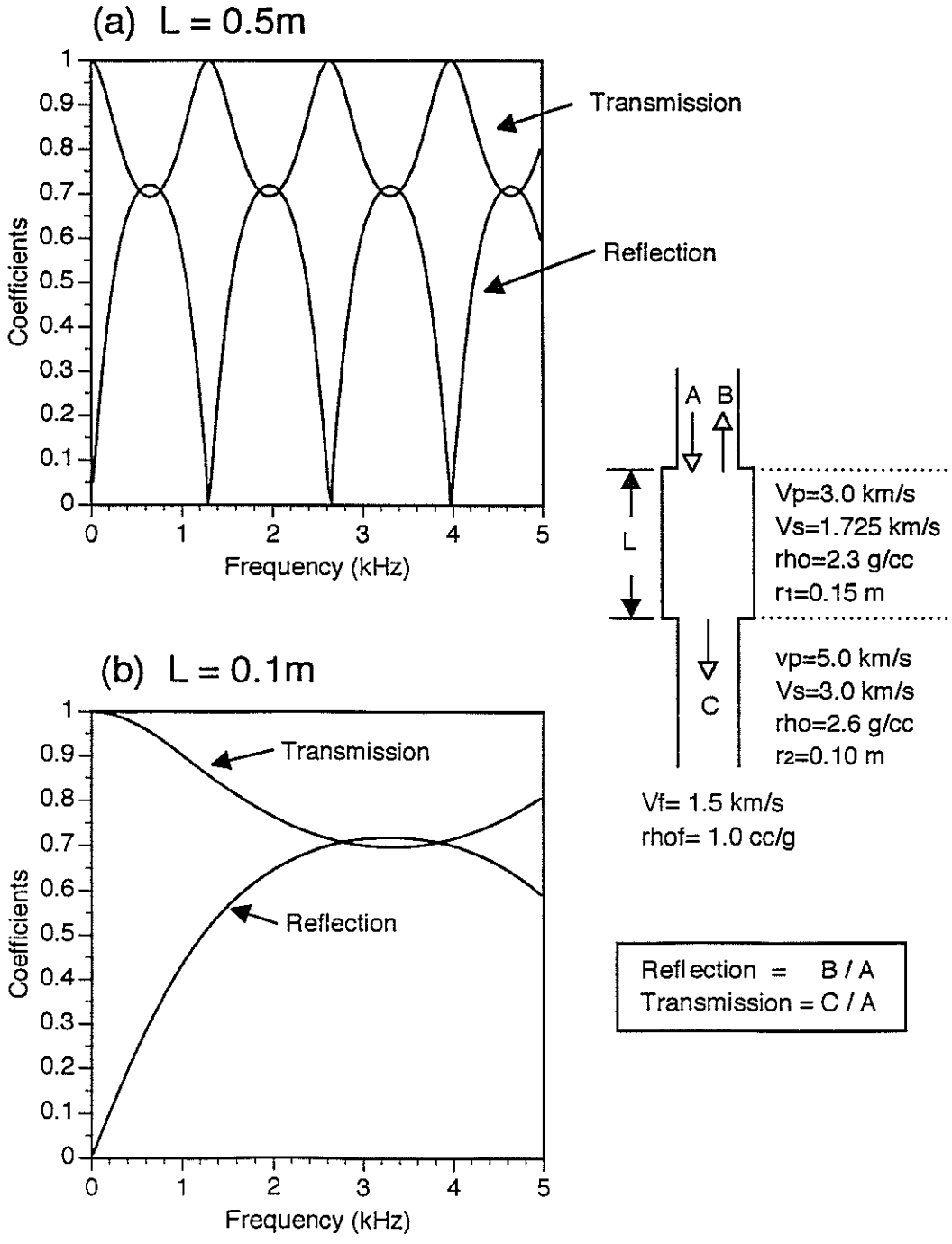

Figure 7: Total transmission and reflection coefficients for a Stoneley wave at washout zones of different thicknesses. (a) Results obtained for the washout zone with a thickness of 0.5m. (b) Results obtained for the washout zone with a thickness of 0.1m. Borehole geometry and model parameters are depicted beside the curves.

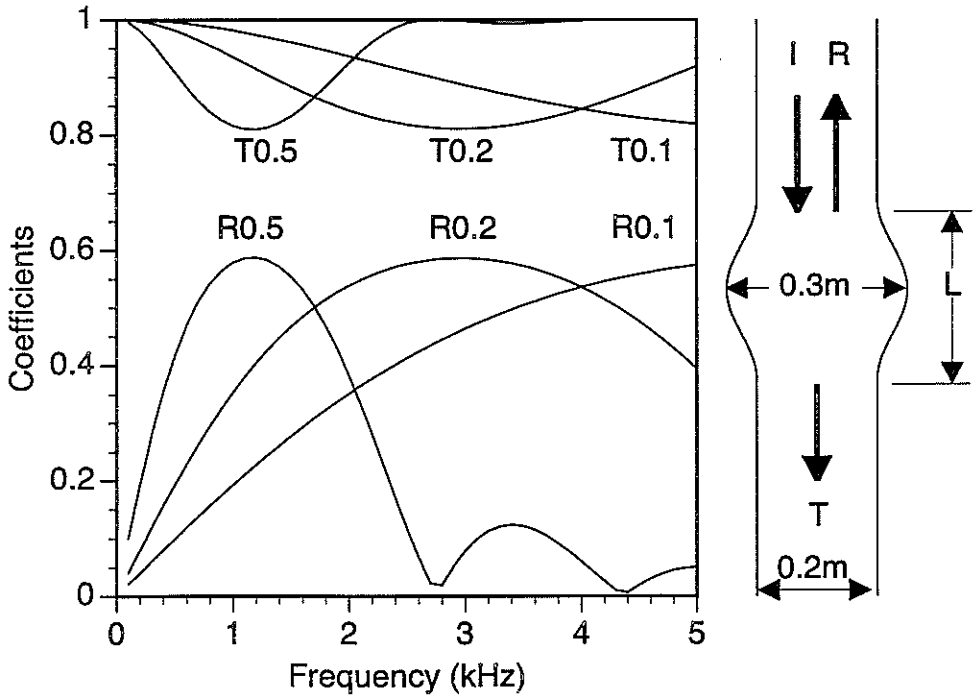

Figure 8: Total transmission and reflection coefficients of a Stoneley wave at sinusoidal washout zones. The zone thicknesses are 0.1m, 0.2m and 0.5m. R0.1 denotes the total reflection for the 0.1m thickness model. T0.5 denotes the total transmission for the 0.5m thickness model.

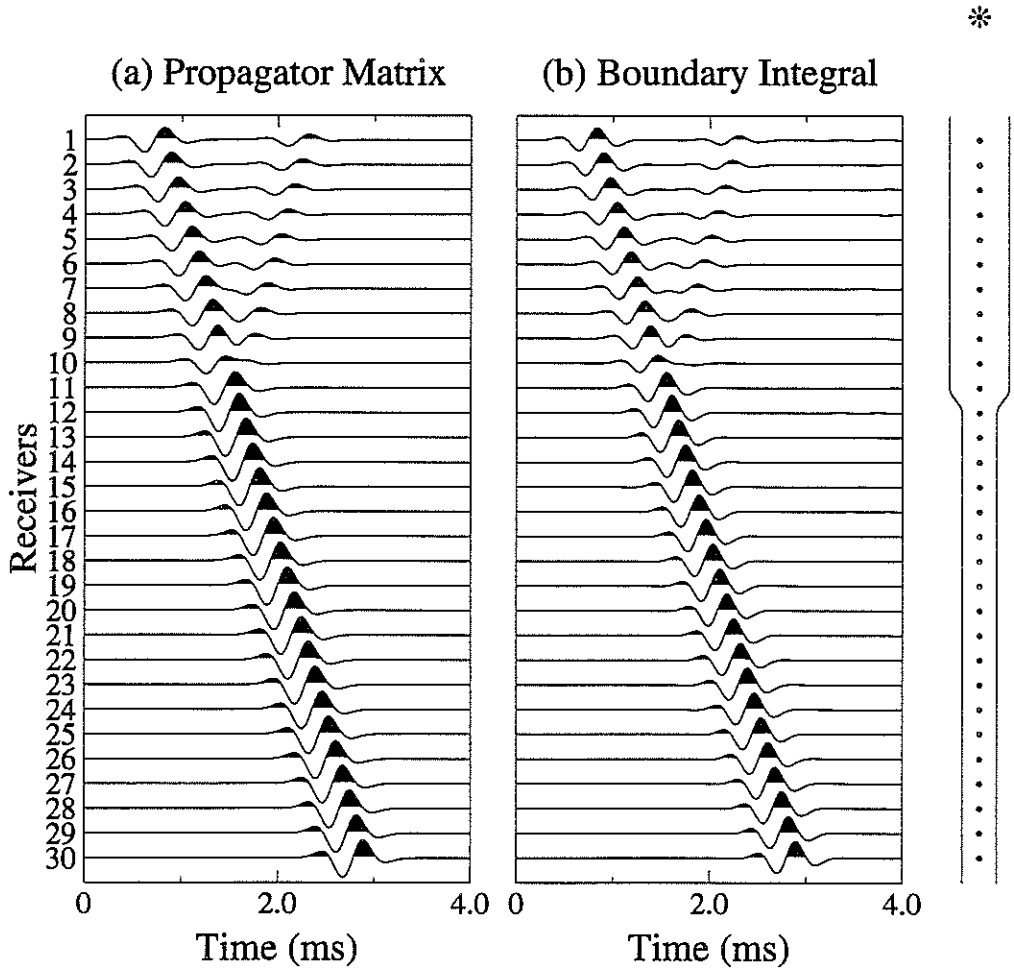

Figure 9: Comparison of the propagator matrix synthetic waveforms (a) with the boundary integral method (b). The steep borehole model, depicted beside the waveforms, has an interval whose radius changes sinusoidally from 12cm at an axial distance of 1.5m from the source to a value of 7cm at the distance of 1.6m. The parameters of the formation and the fluid are the same as those in Figure 3. A Kelly source with a center frequency of 2 kHz is applied as a source. The seismograms recorded by an array of 30 receivers located along the borehole axis at 0.1m interval are displayed.

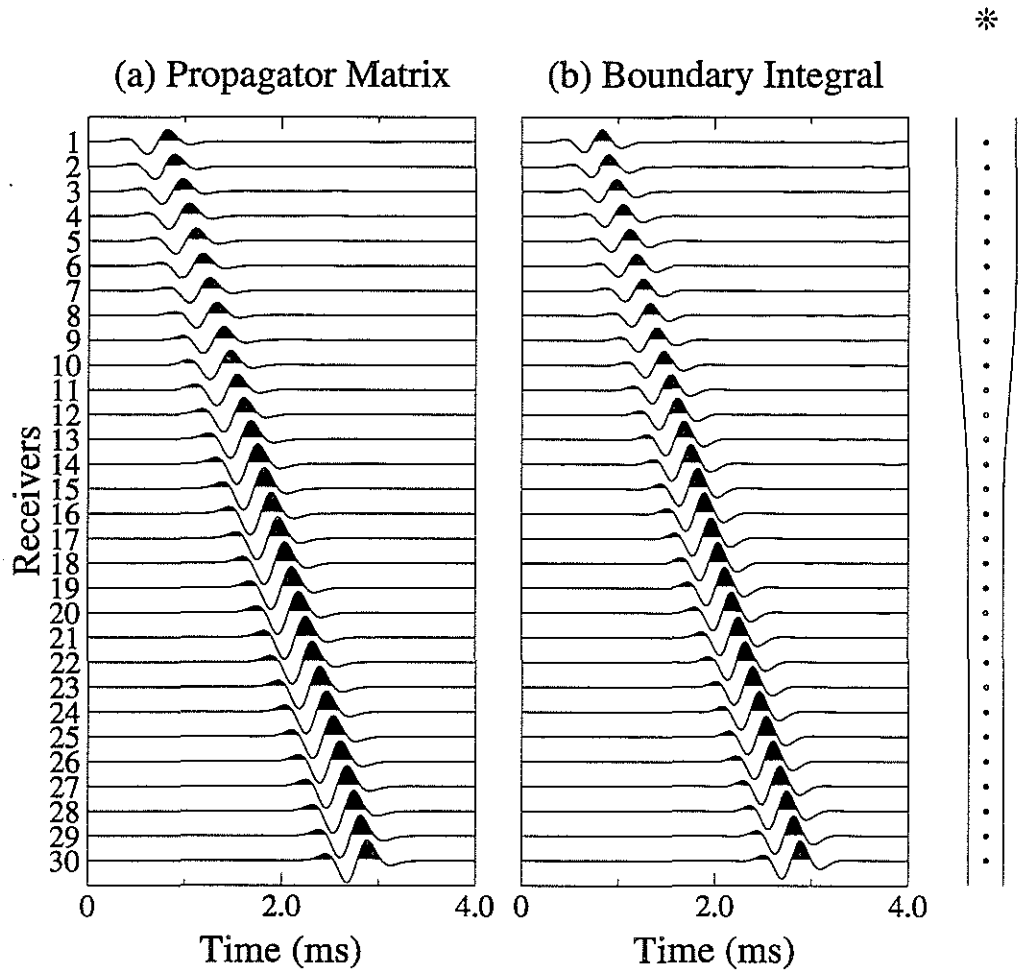

Figure 10: Comparison of the propagator matrix synthetic waveforms (a) with the boundary integral method (b). The smooth borehole model, depicted beside the waveforms, has an interval whose radius changes sinusoidally from 12cm at an axial distance of 1.0m from the source to a value of 7cm at the distance of 2.0m. The parameters of the formation and the fluid are the same as those in Figure 3. A Kelly source with a center frequency of 2kHz is applied as a source. The seismograms recorded by an array of 30 receivers located along the borehole axis at 0.1m interval are displayed.

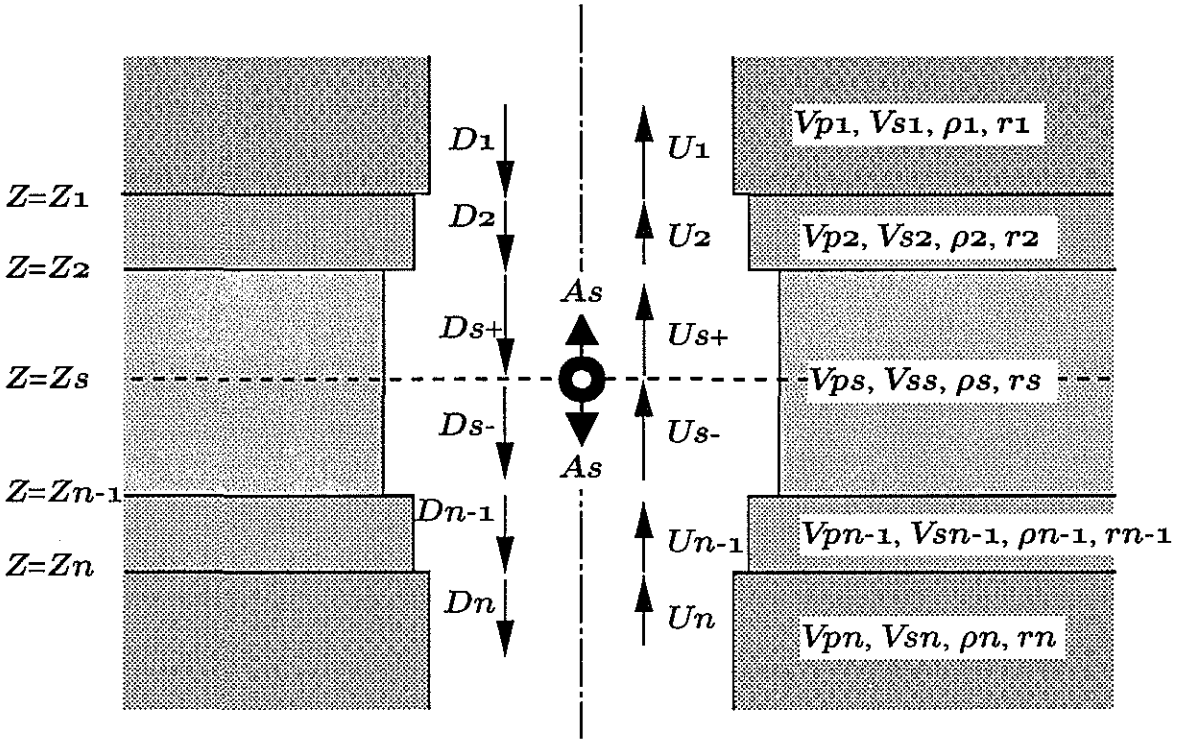

Figure 11: Diagram showing an acoustic source in a washout zone surrounded by multi-layered formation. The Sth layer which includes the source requires special treatment. It is separated into two layers $s+$ and $s-$. U_i and D_i denote amplitudes of up-going and down-going waves in each layer.

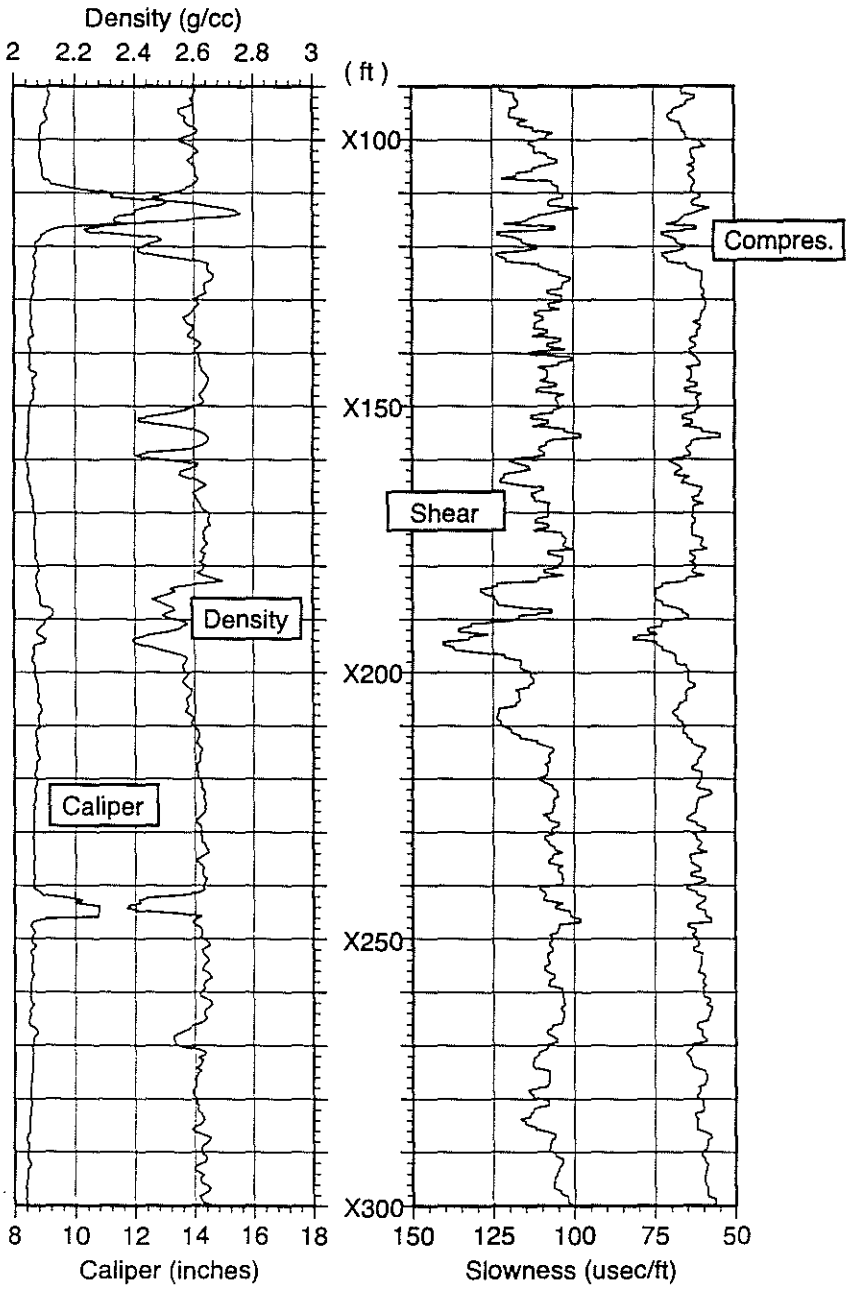

Figure 12: Composite log chart showing profiles of compressional and shear slownesses, formation density and borehole diameter (caliper). These curves are discretized by a one foot interval, and a 560-layer model is made for the synthetic iso-offset records calculation.

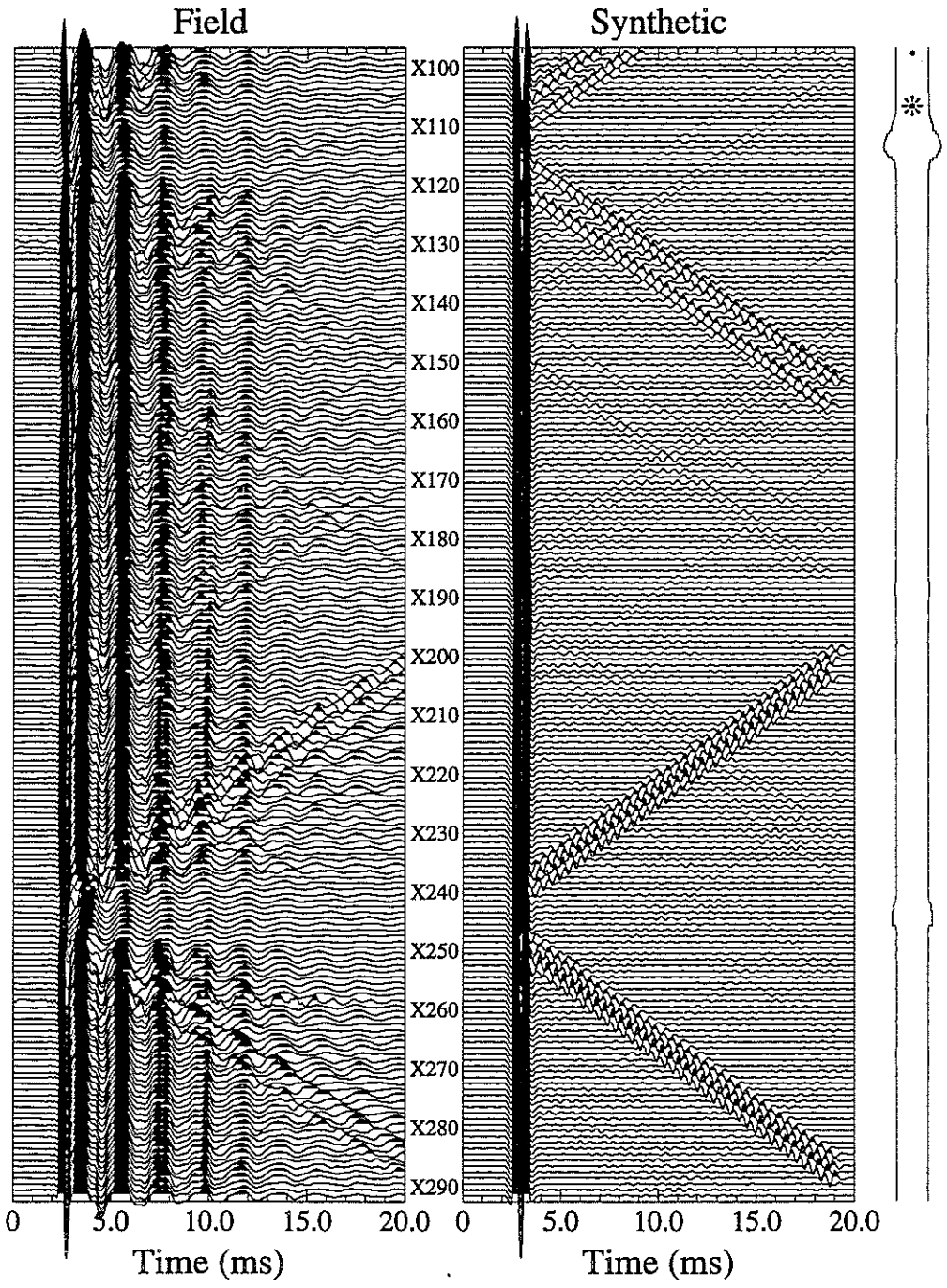

Figure 13: Comparison of the synthetic iso-offset records (b) with the real field records (a). The synthetic records are calculated by the propagator matrix method with the mass balance boundary condition. The model parameters used in the calculation are shown in the composite log chart. The Kelly source with the center frequency of 1.5 kHz is used for the source function.

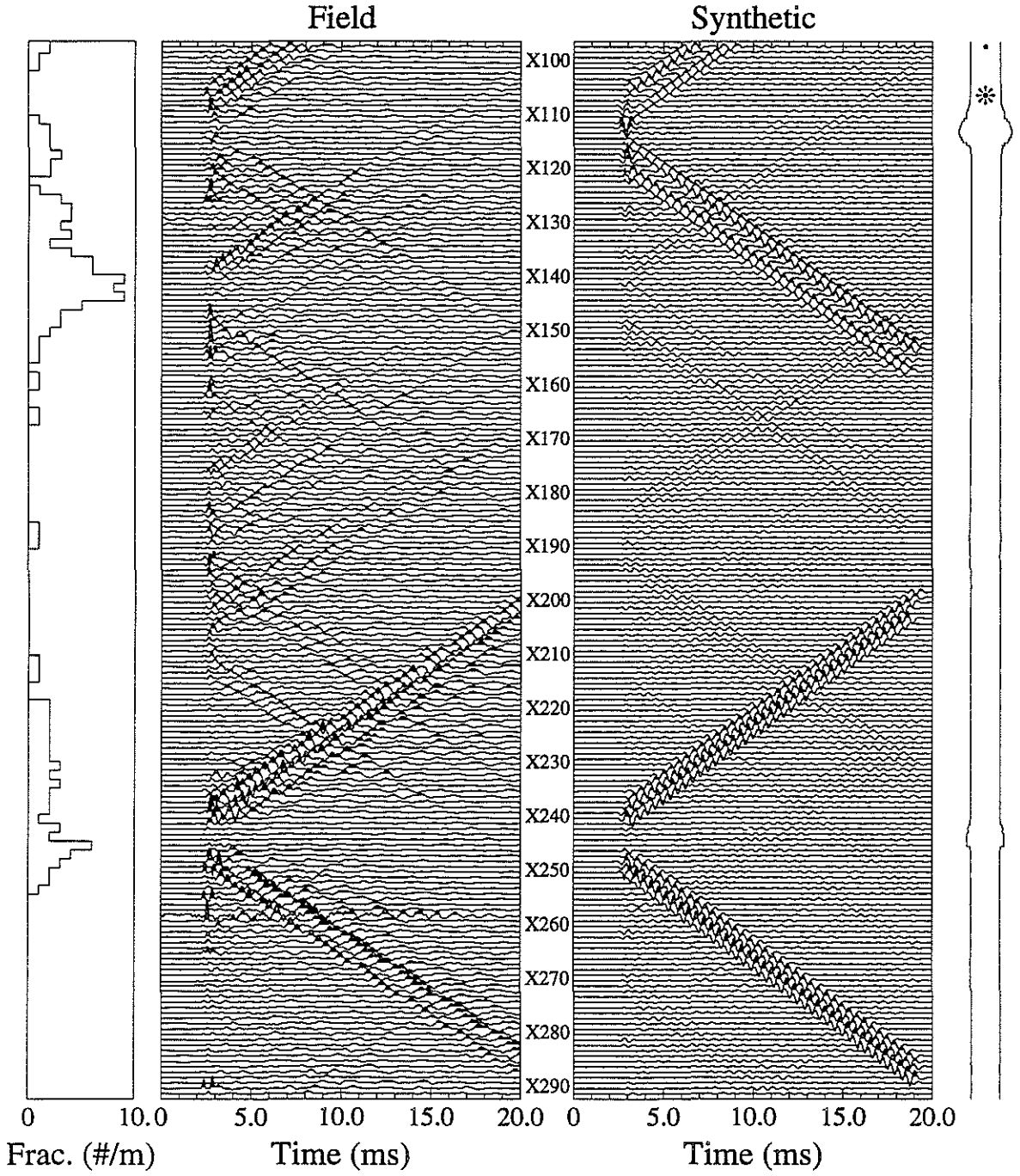

Figure 14: The scattered wavefield of the field records (a) and the synthetic records (b). The median filtering is applied to extract only the scattered wavefield from the total wavefields shown in the preceding figure. The left-hand column shows the fracture density histogram obtained by counting fractures on the resistivity image of the formation micro scanner.